A Large-Droplet Mode and Prognostic Number Concentration of Cloud Droplets in the Colorado State University Regional Atmospheric Modeling System (RAMS). Part I: Module Descriptions and Supercell Test Simulations

STEPHEN M. SALEEBY AND WILLIAM R. COTTON

Colorado State University, Fort Collins, Colorado

(Manuscript received 15 November 2002, in final form 16 August 2003)

ABSTRACT

The microphysics module of the version of the Regional Atmospheric Modeling System (RAMS) maintained at Colorado State University has undergone a series of improvements, including the addition of a large-cloud-droplet mode from 40 to 80 μm in diameter and the prognostic number concentration of cloud droplets through activation of cloud condensation nuclei (CCN) and giant CCN (GCCN). The large-droplet mode was included to represent the dual modes of cloud droplets that often appear in nature. The activation of CCN is parameterized through the use of a Lagrangian parcel model that considers ambient cloud conditions for the nucleation of cloud droplets from aerosol. These new additions were tested in simulations of a supercell thunderstorm initiated from a warm, moist bubble. Model response was explored in regard to the microphysics sensitivity to the large-droplet mode, number concentrations of CCN and GCCN, size distributions of these nuclei, and the presence of nuclei sources and sinks.

1. Introduction

The simulation of cloud microphysics in mesoscale and cloud-resolving models can be done by following either a full bin-resolving approach or a bulk microphysics approach. In the former, the hydrometeor size spectra are explicitly resolved in a set of bins. For liquid clouds, this approach can involve as many as 70 or more bins in a single-moment scheme or 30 or more bins in a two-moment scheme (Berry 1967; Tzivion et al. 1987; Kogan 1991). This approach requires large amounts of computational time and memory, and, thus, the bin-resolving approach is generally limited to simple cloud systems (e.g., Kogan 1991; Feingold et al. 1988; Ovtchinnikov and Kogan 2000). As a result, most mesoscale and storm models use the bulk microphysics approach. This approach follows the lead of Kessler (1969) in which the liquid drop spectrum is partitioned between cloud droplets and raindrops. Raindrops are assumed to be distributed in an exponential, or Marshall–Palmer, spectrum, which forms from collected cloud droplets by continuous accretion. The initial formation of raindrops is parameterized by what is called an autoconversion process. Kessler hypothesized a simple linear relationship as a function of cloud liquid water content for autoconversion. Manton and Cotton (1977) used simple dimensional analysis arguments to extend this concept to include the influence of varying cloud droplet concentrations. A number of researchers have used a more formal approach in which simple closed-box calculations are used to form empirical autoconversion parameterizations (Berry 1967, 1968; Cotton 1972; Berry and Reinhardt 1974). A more sophisticated approach is that of Khairoutdinov and Kogan (2000), who derived an autoconversion parameterization from the statistical analysis of large-eddy simulations (LES) of the stratus-topped marine boundary layer with bin-resolved microphysics. The scheme was then tested in the LES framework against LES with bin-resolved microphysics. Another feature of their scheme is that cloud condensation nuclei (CCN) activation and sources and sinks are explicitly parameterized, whereas other autoconversion schemes simply use CCN concentration as being the same as droplet concentration.

Most mesoscale models like the fifth-generation Pennsylvania State University–National Center for Atmospheric Research Mesoscale Model (MM5; Hsie and Anthes 1984; Dudhia 1989), the Advanced Regional Prediction System (ARPS; Souto et al. 2003), the Goddard Cumulus Ensemble (GCE; Tao et al. 1989), and the Weather Research and Forecasting model (WRF; Hong et al. 1998; Zhao and Carr 1997) follow the above Kessler paradigm with extensions to ice-phase clouds that generally follow Lin et al. (1983) and Rutledge and Hobbs (1983). Only a single moment, such as the mixing ratio of each hydrometeor species, is generally predict-

Corresponding author address: Stephen M. Saleeby, Atmospheric Science Department, Colorado State University, Fort Collins, CO 80523.
E-mail: smsaleeb@atmos.colostate.edu

ed. It has become more common in recent years for bulk microphysics schemes to predict two moments, such as the hydrometeor mixing ratio and concentration (Ferrier et al. 1995; Meyers et al. 1997; Reisner et al. 1998). A somewhat different paradigm is to emulate an explicit bin model by prescribing basis functions for the drop size distributions, such as gamma or lognormal distributions (Clark 1976; Clark and Hall 1983), and to predict explicitly the evolution of those basis functions by vapor deposition/evaporation, stochastic coalescence, and sedimentation. Tzivion et al. (1994) predict three parameters that fully define the basis functions: mixing ratio, number concentration, and median radius. The parameterization scheme we describe in this paper follows the latter paradigm.

Our motivation for developing a new microphysics parameterization in the Regional Atmospheric Modeling System (RAMS) developed at Colorado State University (CSU) came from Verlinde et al. (1990), who showed that analytical solutions to the collection equation were possible when applied to predictions of the hydrometeor mixing ratio and concentrations. They showed that solutions to the full stochastic collection equation can be obtained if the collection efficiencies are held constant. This approximation is also typically used in classical bulk parameterization schemes that follow Kessler's (1969) basic approach. Walko et al. (1995) describe the implementation of this approach in RAMS for prediction of hydrometeor mixing ratios. An important aspect of the implementation strategy was the use of lookup tables that enabled fast and accurate solutions to the collection equations. Meyers et al. (1997) then extended this approach to two moments of the hydrometeor spectra: mixing ratio and number concentration. Also, in Verlinde et al. (1990) and subsequent implementations in RAMS, the Kessler-type exponential or Marshall–Palmer basis function for hydrometeor spectra was abandoned in favor of a generalized gamma distribution function,

$$n(D) = \frac{N_t}{\Gamma(\nu)}\left(\frac{D}{D_n}\right)^{\nu-1}\frac{1}{D_n}\exp\left(-\frac{D}{D_n}\right), \qquad (1)$$

where $n(D)$ is the number of particles of diameter D, N_t is the total number of particles, ν is the shape parameter, and D_n is some characteristic diameter of the distribution. The Marshall–Palmer (exponential) and Khrgian–Mazin distribution functions are special cases of this generalized function. Owing to the use of lookup tables, it became apparent that it is no longer necessary to constrain the system to constant or average collection efficiencies. Thus, Feingold et al. (1988) replaced the formerly ad hoc autoconversion formulations in RAMS with full stochastic collection solutions for self-collection among cloud droplets and for rain (drizzle) drop collection of cloud droplets. The lookup tables were then computed using realistic collection kernels from Long (1974) and Hall (1980) rather than constant collection efficiencies used in earlier versions of RAMS. The philosophy of bin representation of collection was also extended to calculations of drop sedimentation. Bulk microphysics schemes have previously treated sedimentation of hydrometeors by integrating over the entire particle size spectra and obtaining a mass-weighted fall speed. The closest agreement between a full bin-resolving microphysics model in an LES of marine stratocumulus cloud and the bulk microphysics representation was obtained (Feingold et al. 1999) when both collection and sedimentation were simulated by emulating a full-bin model with 36 bins. Bin sedimentation is simulated by dividing the gamma distribution into discrete bins and then building lookup tables to calculate how much mass and number in a given grid cell fall into each cell beneath a given level in a given time step.

Up to this point, the model did not explicitly represent the nucleation of cloud droplets on specified or predicted CCN. CCN was used as an input variable to define the concentration of cloud droplets, but explicit nucleation and vapor growth were not represented. The cloud droplet spectrum mentioned here was also limited in its size range from about 2 to 40 μm in diameter. The next size of liquid hydrometeor species was the rain category, which is considerably larger than these droplets. To improve these limitations to the RAMS model, explicit nucleation of cloud droplets via parameterized activation of CCN and/or giant CCN (GCCN) has been added, as well as a second cloud mode of large cloud droplets with diameters from 40 to 80 μm. The 40-μm division between the two modes is natural because it is well known that collection rates for droplets smaller than this size are very small, whereas droplets greater than this size participate in vigorous collision and coalescence (Pruppacher and Klett 1997). Moreover, the new large-cloud-droplet mode, in combination with the traditional single mode of cloud droplets, permits representation of the bimodal distribution of cloud droplets that is often seen in clouds (Hobbs et al. 1980). The introduction of prognostic number concentration of cloud droplets, through activation of CCN and growth of solution droplets, provides a more physically consistent calculation of the amount of droplet mass and number.

The new droplet category joins the seven other hydrometeor species that are accounted for in RAMS. These are as follows: small cloud droplets, large cloud droplets, rain, pristine ice, snow, aggregates, graupel, and hail. The large-cloud-droplet mode (hereinafter referred to as cloud2) is allowed to interact with all other species, similar to the small-droplet mode (hereinafter referred to as cloud1). Cloud2 plays a significant role in the collision–coalescence process by requiring droplets to grow at a slower rate as they pass from cloud1 to rain, rather than being transferred directly from cloud1 to rain. There is also a significant impact by cloud2 upon ice formation, because two modes now exist and are allowed to participate in homogeneous freezing nucleation, secondary ice production through

the Hallett–Mossop processes, and collisions with ice species. Prognostic number concentration of both cloud modes has been also been introduced into the model microphysics. This introduction was made possible through use of a Lagrangian parcel model, which is discussed in Heymsfield and Sabin (1989) and Feingold and Heymsfield (1992). The parcel model has made it possible to construct lookup tables, for use in the RAMS cloud droplet nucleation routine, that predict the percent of CCN to activate, depending upon model atmospheric conditions. CCN (GCCN) are assumed to be ammonium sulfate (sodium chloride) particles that activate and grow by vapor diffusion into cloud1 (cloud2) droplets.

Sensitivity tests have been performed in three-dimensional, homogeneous, idealized convective environments that were initiated with a warm bubble and a convective sounding. Such tests were performed to examine the model sensitivity to variations in the cloud droplet spectrum, CCN and GCCN number concentrations, and the treatment of aerosol sources and sinks.

2. Lagrangian parcel model

The Lagrangian parcel model (Heymsfield and Sabin 1989; Feingold and Heymsfield 1992) approach used in the prediction of cloud droplet nucleation follows the Köhler equations and cloud droplet growth formulation from Pruppacher and Klett (1997, 506–513). The parcel model is activated with user-specified environmental conditions and a CCN population; the model performs time integrations of droplet formation and growth as it lifts an individual parcel, thereby allowing CCN to deliquesce, activate, and grow from haze particles to cloud droplet sizes. The percentage of CCN that result in the formation of cloud droplets is then used in the parameterization of cloud droplet formation in the mesoscale RAMS.

The parcel model solves the set of ordinary differential equations that define the microphysics of cloud droplet growth from deliquesced aerosol and the dynamical influence of a rising parcel of air. Starting at time zero, a parcel that contains a distribution of dry CCN is deliquesced and lifted by an established vertical velocity and time step interval. The variable coordinate ordinary differential equation (VODE) solver (Brown et al. 1989) proceeds through the following equation set to solve iteratively the droplet growth equation while considering the time rate of change of the saturation ratio, temperature, air and droplet solution density, liquid water content, and air pressure of the parcel during lifting.

From a given number concentration and median radius of CCN, the parcel model represents the CCN spectrum as a binned lognormal distribution:

$$N(r) = \frac{N_t}{r\sqrt{2\pi}\,\ln\sigma}\exp\left\{\frac{-[\ln(r/r_g)]^2}{2(\ln\sigma)^2}\right\}. \quad (2)$$

Here, r is the bin radius, $N(r)$ is the number concentration of CCN for a given radius bin, N_t is the total number concentration of CCN, σ is the distribution breadth parameter, and r_g is the distribution median radius. This distribution breaks up the total CCN number concentration into 200 mass bins ranging from 10^{-17} to 10^{-8} g, with a distribution breadth of $\sigma = 1.8$. Bin radii are diagnosed from the mass and density of the solute mass; the CCN are assumed to consist of ammonium sulfate, with a dry density $\rho_{\text{ccn}} = 1.769(\text{g cm}^{-3})$. A formulation is first needed for initial growth by vapor diffusion from a dry CCN distribution to a distribution of solution droplets in supersaturated conditions. The model first represents deliquescence of CCN from the dry distribution by establishing a distribution of solution droplets that are unactivated and in equilibrium at the given initial saturation ratio. The model assumes that the unlifted parcel has been at the initial, unsaturated relative humidity long enough for soluble material to deliquesce and reach equilibrium diameters. This assumption is not particularly unreasonable for generally small CCN (Pruppacher and Klett 1997). The unactivated spectrum of solution droplets in equilibrium with an initial subsaturated relative humidity is calculated iteratively from the following form of the Köhler equation:

$$S_{v,w} = \frac{e_r}{e_{\text{sat},w}} = \exp\left[\frac{2M_w\sigma_{s/r}}{\Re T\rho_w r} - \frac{\nu\phi_s\varepsilon M_w\rho_{\text{ccn}}r_0^3}{\rho_w M_s(r^3 - r_0^3)}\right], \quad (3)$$

in which $S_{v,w}$ is the saturation ratio, e_r is the vapor pressure over the solution droplet, $e_{\text{sat},w}$ is the saturation vapor pressure over water, M_w is the molecular weight of water, $\sigma_{s/r}$ is the surface tension of the solution droplet, $\Re$ is the universal gas constant, T is ambient temperature, ρ_w is the density of water, ε is the fraction of CCN soluble material, r is the equilibrium radius of the solution droplet, r_0 is the dry radius, ν is the number of ions into which an ammonium sulfate molecule dissociates, ϕ_s is the molal osmotic coefficient, and M_s is the molecular weight of the solution constituent. The value of $\nu\phi_s$ was determined from a polynomial fit to the values of the van't Hoff factors from Low (1969) for an ammonium sulfate composition at $+25°$C and 1atm.

Upon computation of the equilibrium droplet diameters, the model initiates a time integration of the following set of equations to determine the solution droplet growth rate for the given ambient conditions. The given parcel is lifted at 5-m increments from 300 up to 50 m beyond the point at which maximum supersaturation is reached. The model time step is computed as the vertical grid spacing divided by the given vertical velocity; thus, this time step will vary as the model is run for different vertical velocities. As the parcel is lifted, the droplet growth equation determines the evolution of droplet sizes for each bin in the CCN distribution. For each mass bin, the growth equation is calculated as

$$r\frac{dr}{dt} = \frac{s_{v,w} - y}{\dfrac{\rho_w \Re T}{e_{\text{sat},w} D_v^* M_w} + \dfrac{L_v \rho_w}{k_r^* T}\left(\dfrac{L_v M_w}{T\Re} - 1\right)}, \quad (4)$$

where $S_{v,w}$ is the supersaturation, T is the ambient temperature, L_v is the latent heat of vaporization, D_v^* is the modified diffusivity, and k_r^* is the modified thermal conductivity. The y term considers curvature and solute effects and is given as

$$y = \frac{2M_w\sigma_{s/r}}{\Re T \rho_w r} - \frac{\nu\phi_s\varepsilon m_s M_w/M_s}{(4\pi r^3\rho_s/3) - m_s}, \quad (5)$$

in which ρ_s is the droplet solution density. The diffusivity and thermal conductivity, modified to consider gas kinetic effects, are

$$D_v^* = \frac{D_v}{\left[\dfrac{r}{r + \Delta_v} + \dfrac{D_v}{r\alpha_c}\left(\dfrac{2\pi}{R_v T_r}\right)^{1/2}\right]} \quad \text{and}$$

$$k_a^* = \frac{k_a}{\left[\dfrac{r}{r + \Delta_T} + \dfrac{k_a}{r\alpha_T \rho c_p}\left(\dfrac{2\pi}{R_v T_r}\right)^{1/2}\right]}. \quad (6)$$

The coefficients Δ_v and Δ_T are the vapor and thermal jump lengths that vary with temperature and pressure, $\alpha_c = 0.042$ and $\alpha_T = 0.96$ are the condensation and thermal accommodation coefficients, ρ is the moist air density, c_p is the specific heat at constant pressure, and R_v is the water vapor gas constant. At the initial model start, the droplet growth equation is calculated from the initial values for pressure, temperature, and saturation. The model then computes the time derivatives of the solution density and air density, respectively, as

$$\frac{d\rho_s}{dt} = \frac{3}{r}\frac{dr}{dt}(\rho_w - \rho_s) \quad \text{and}$$

$$\frac{d\rho}{dt} = \frac{T\dfrac{dp}{dt} - p\dfrac{dT}{dt}}{R_d T^2}, \quad (7)$$

in which p is air pressure and R_d is the dry gas constant. The derivative of the droplet spectrum liquid mixing ratio, dX_L/dt, is then computed by reformulating the droplet growth equation to represent the mass growth rate and then summing the mass calculation over all distribution bins. Calculating dX_L/dt in this manner accounts for the possibility that some of the droplets in the large mass bins are not yet at equilibrium (Heymsfield and Sabin 1989). In this manner, the parcel model will account for the length of time needed for solution droplets of differing sizes to potentially activate and grow. Upon computation of the derivative of liquid mixing ratio, the time derivative of the saturation ratio of the ascending parcel can be determined as

$$\frac{ds}{dt} = sgw\left(\frac{L_v}{R_v T^2 c_p} - \frac{1}{R_d T}\right) - s\rho\left(\frac{R_d L_v^2}{pR_v T c_p} + \frac{R_v T}{e_{\text{sat},w} s}\right)\frac{dX_L}{dt}, \quad (8)$$

where g is gravity and w is the vertical velocity. The first term is the vapor contribution from parcel lifting and the second term is the vapor that is depleted from droplet growth. The time derivative of parcel temperature during ascent is also a function of the derivative of liquid mixing ratio; it is assumed to undergo dry adiabatic lifting and is influenced by latent heat release from vapor condensation:

$$\frac{dT}{dt} = \frac{L_v}{c_p}\frac{dX_L}{dt} - \frac{gw}{c_p}. \quad (9)$$

Within the same time step, $d\rho/dt$ and dX_L/dt are then recalculated from the updated value of dT/dt; these new values then feed into recalculations of ds/dt and dT/dt as the final time step adjustment. This equation set is solved iteratively for each time step, using the VODE solver. This process is repeated in the model for successive time steps and vertical intervals until the maximum supersaturation is reached. Once the parcel has reached maximum supersaturation, it is allowed to lift another 50 m to allow time for CCN activation. Beyond the point of maximum supersaturation, the rate of vapor diffusion toward solution droplets matches or exceeds the rate of vapor supply from the lifting of the parcel. The given number of activated droplets is then computed to determine the percentage of initial CCN that deliquesce, activate, and grow to cloud droplet diameters greater than 2 μm.

Within the parcel model integrations, a number of assumptions are necessary to limit the degrees of freedom and the subsequent lookup-table array dimensions. Upon extensive testing, it was decided to allow the model realizations to vary in four dimensions with temperature, vertical velocity, concentration of CCN, and median radius of the CCN distribution. The distribution breadth parameter, initial relative humidity, ambient air pressure, and CCN chemistry were held constant because these produce the least relative variability in the results. Tests of various initial relative humidity values from 85% to 99% result in only small variations in the final percentage of activated CCN in comparison with the dependence of the free variables mentioned above. The resulting cloud droplet nucleation lookup table is arranged as a four-dimensional data array that contains the percentage of CCN that activate in the parcel and grow to the minimum cloud droplet size. Each of the four dimensions (temperature, vertical velocity, CCN concentration, and CCN median radius) is varied in the parcel model, which results in varying percentages of CCN that eventually form cloud droplets.

At the outset of the parcel model, the free variables

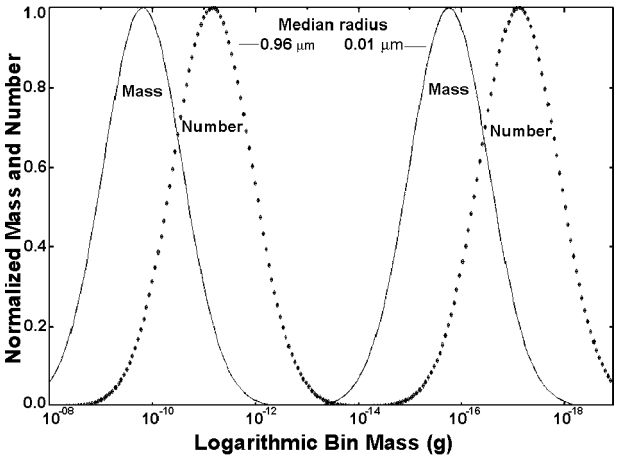

FIG. 1. Normalized CCN mass and number distribution on a log-normal scale. Plot displays the maximum and minimum median radii allowed for CCN in RAMS. Distributions for different radii are similar except displaced along the CCN mass scale. Note the difference in bin location between the peaks of the concentration of mass and number for a given radius. The largest amount of number is located in the smaller mass bins.

were run over the following range of possible atmospheric values: CCN concentration from 10 to 10 000 cm^{-3}, vertical velocity from 0.01 to 100 m s^{-1}, temperature from $-30°$ to 30°C, and CCN median radius from 0.04 to 0.96 μm. The initial pressure was fixed at 600 hPa, and the initial relative humidity was set at 99%. Figure 1 shows the normalized distributions of CCN mass and number versus bin mass for the range of median radius. Parcel model results reveal that the largest *percentage* of CCN result in droplet formation under conditions of low temperature, strong updraft velocity, large median radius, and small CCN number concentration. Figure 2 displays plots of these results in which each of the four variables was allowed to vary in increments over its range while the other variables were held constant at a midrange atmospheric value.

The plot of temperature dependence is somewhat misleading because it should be expected that equilibrium droplet sizes and growth rate should be greater at warmer temperatures. This would be the case for stationary growth, but the parcel considered here is being lifted to the point at which maximum supersaturation occurs. There are competing effects for CCN activation between the supersaturation needed to keep a solution drop at equilibrium [Eq. (3)] and the time rate of change of supersaturation with height as a parcel is initially lifted

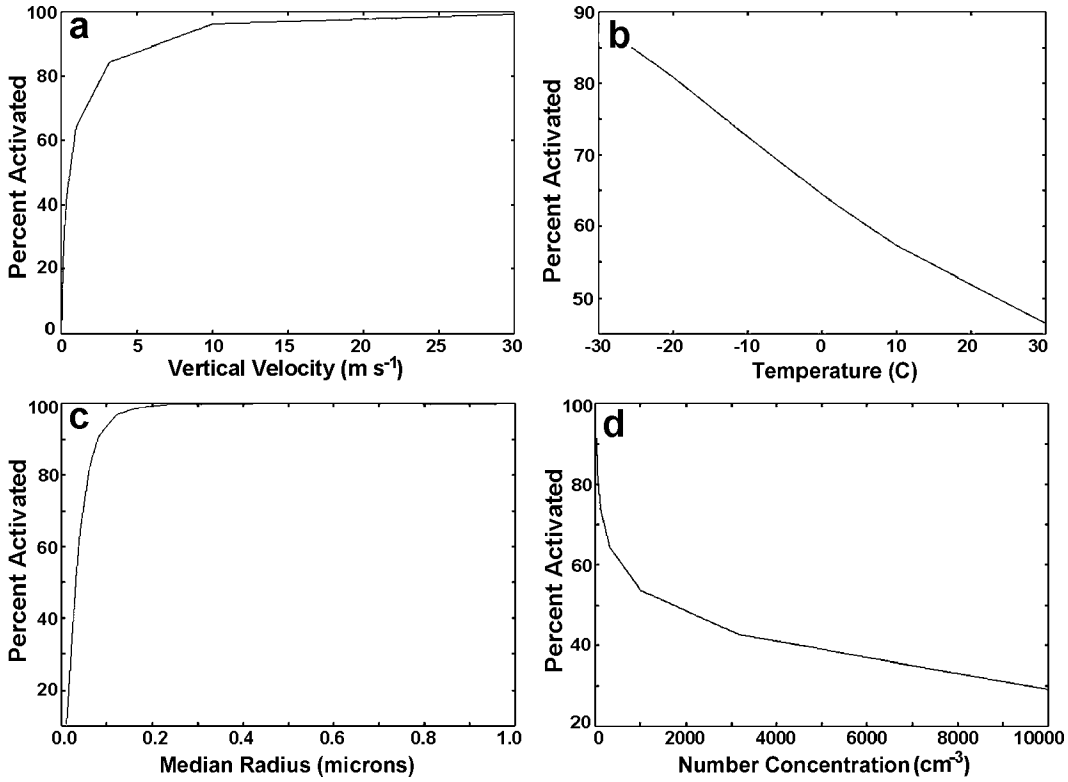

FIG. 2. Variations in the percent of CCN that are activated depending upon the (a) vertical velocity, (b) temperature, (c) median radius of CCN spectrum, and (d) CCN concentration. For each variation, the other variables were held fixed at the following values: vertical velocity = 1 m s^{-1}, concentration = 300 cm^{-3}, median radius = 0.04 μm, and temperature = 0°C.

[Eq. (8)]. As the temperature decreases, the supersaturation needed to keep a solution drop at equilibrium increases, but the time rate of change of supersaturation of a lifted parcel also increases. Equation (8) varies as T^{-2} while Eq. (3) varies at T^{-1}; thus, the rate of change of supersaturation is the dominant factor here, and we see higher supersaturations and greater percentages of CCN being activated at lower temperatures. As a result, a colder parcel is lifted over a greater depth before maximum supersaturation is reached. In the absence of very strong vertical velocity, a lifted parcel typically reaches its maximum supersaturation within 100 m of the cloud base. The increased supersaturation and lifting in colder conditions allows more CCN to be activated and grow by vapor diffusion into cloud droplets.

The inclusion of the variable median radius is a necessary addition to the parcel model because it drastically affects the percent of CCN that activate. This allows for shifting of the nuclei spectrum in RAMS to smaller sizes upon activation of the larger aerosol, which results in a decrease in percentage of possible CCN to activate. It also allows a shifting of the spectrum to larger sizes upon evaporation of liquid droplets and restoration of CCN. The median radius (r_g) can be approximated by the following equation in which ρ is the density of the solute mass of CCN or GCCN, N is the number concentration (cm^{-3}), and m is the total mass (g):

$$r_g = \left[\frac{3}{4}\frac{1}{\rho\pi}\frac{m}{Ne^{(\pi/2)}}\right]^{1/3}. \tag{10}$$

The parcel model was also run for GCCN with median radii from 1 to 5 μm and concentrations from 10^{-5} to 10^{-1} cm^{-3}. Results reveal that nearly all deliquesced GCCN activate and grow as solution droplets to sizes beyond the cloud droplet threshold size for all environmental conditions allowed in the model; thus, lookup tables are unnecessary. The underlying assumption here is that all GCCN will deliquesce and reach equilibrium; this assumption is problematic because the time required for nuclei to reach equilibrium increases with increasing size. Despite the relatively long time needed for GCCN activation, it has been shown that the presence of GCCN is highly influential in rain formation, especially in clouds that are very colloidally stable (e.g., Johnson 1982; Tzivion et al. 1994; Cooper et al. 1997; Feingold et al. 1999). Large-sized GCCN were shown to accelerate and to participate actively in collision–coalescence with existing cloud droplets, thereby leading to a more rapid broadening of the droplet spectrum and transition to rain. The large end of the GCCN distribution used here would effectively participate in collision–coalescence, and the small end of the distribution would, indeed, have enough time to reach equilibrium. Because we currently cannot account for the time factor in GCCN reaching equilibrium and we cannot account for GCCN collision–coalescence, we must assume in the meantime that GCCN have reached equilibrium size if we want to include the influence of GCCN in the model.

3. RAMS microphysics enhancements

a. General RAMS modifications

Within the RAMS microphysics, the cloud2 mode was added as a new microphysics hydrometeor species with a diameter from 40 to 80 μm. Because the cloud2 mode is not considerably larger than the cloud1 mode (2–40 μm in diameter), it makes use of the cloud1 mass and fall-velocity power-law relations and the mass-dependent equations for calculating the collection efficiency of droplet–ice collisions. The cloud2 droplets are also considered large enough to participate in the Hallett–Mossop ice-splintering process (Hallett and Mossop 1974). The RAMS ice-splintering parameterization, described in Cotton et al. (2003), is based on an empirical formula from Mossop (1978) that depends upon the number concentrations of cloud droplets greater than 24 and less than 13 μm in diameter. The cloud2 mode is considered in the condensation, evaporation, bin sedimentation, and homogeneous freezing processes; these droplets are considered to be small enough that droplet temperature can be diagnosed from a heat balance equation rather than from individual internal heating calculations (Walko et al. 2000).

b. Large-droplet mode and collision–coalescence

The binned collection process in RAMS uses the mass doubling of bins from Tzivion et al. (1987). For liquid-phase hydrometeors, the following collisions are possible: cloud1–cloud1, cloud1–cloud2, cloud2–cloud2, cloud1–rain, cloud2-rain, and rain–rain. The cloud1-mode diameter extends to 40 μm (bins 1–11), cloud2 extends from 40 to 80 μm (bins 12–15), and rain is greater than 80 μm (bins 16–36). Because cloud2 comprises the fewest bins, the mass within this range still remains relatively small in comparison with the other two liquid species. Figure 3 provides a view of the three spectra of liquid hydrometeors. Inclusion of the cloud2 mode now requires that cloud1–cloud1 collisions must first enter the cloud2 mode instead of directly entering the rain category. Cloud1–cloud 2 and cloud2–cloud2 collisions can directly enter the rain category. Cloud1 droplets that engage in the collision–coalescence process will begin growing and will be forced to enter the cloud2 category before transferring to rain. This requirement tends to slow the growth rate into rain and, therefore, delays the onset of precipitation and limits the surface accumulation of rain.

c. CCN and giant-CCN degrees of freedom

RAMS now has available the options for both one- and two-moment prediction for the cloud1 and cloud2

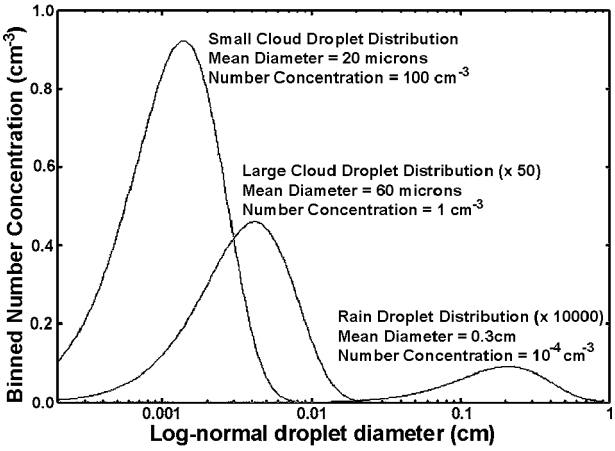

FIG. 3. Droplet spectra for the rain and dual-cloud-droplet hydrometeor categories. For comparison with the small-cloud-droplet mode, the number concentration for the given diameter is exaggerated for the rain and large-cloud-droplet modes.

categories. The new two-moment prediction considers formation of cloud1 (cloud2) droplets by activation and vapor growth of CCN (GCCN). With one-moment prediction of cloud2, acquisition of the cloud2 mixing ratio comes solely from hydrometeor transfers by collision–coalescence. This limit slows the transitional growth from cloud1 to rain by providing this intermediate category. In the two-moment prediction of cloud2, GCCN activate and grow to enter the large-droplet category, which tends to speed up the production of rain because these droplets are already of appreciable size.

CCN and GCCN are also allowed another degree of freedom concerning source and sink options. Nuclei may be treated with one of the following options: 1) nuclei number and mass can remain constant throughout a simulation, 2) nuclei can deplete their source upon activation, or 3) nuclei can both deplete upon activation and reform upon evaporation of liquid hydrometeors. When CCN deplete and/or replenish, the available nuclei mass is tracked so that the median radius can be recalculated at each time step. When considering dissolved nuclei within hydrometeors, only the mass is tracked because this parameter is conserved after droplet formation; number concentration can be diagnosed upon liquid hydrometeor evaporation. Upon droplet evaporation, the model determines the number of droplets that evaporate and the liquid water that returns to the vapor state. Because CCN are only restored upon the complete evaporation of a droplet, the model computes the number of totally evaporated droplets and the corresponding liquid water. The ratio of liquid water in the totally evaporated droplets to the total cloud droplet water content is determined, and then this ratio is used to return a corresponding amount of dissolved CCN mass contained with the hydrometeors. Each evaporated cloud droplet simply produces one CCN back to the atmosphere. From the restored mass and number, the median radius of the restored droplets can be calculated from Eq. (10).

d. Activation process for CCN and giant CCN

If both cloud1 and cloud2 are predicted with two moments, and CCN and GCCN are allowed to deplete upon activation and replenish upon liquid hydrometeor evaporation, then the following process occurs. At the first time step, the cloud droplet nucleation routine obtains the user-specified field of nuclei (cm^{-3}) and the median radius of the distribution. The user may specify the number concentration with a single value that creates a homogeneous field, a vertical profile, or a 3D heterogeneous field that can be vertically and horizontally advected and diffused. From the radius and CCN number concentration, the CCN mass can be calculated from the nuclei-spectrum lookup tables.

The nuclei-spectrum lookup tables are essentially lognormal distributions of CCN/GCCN, given the median radius, number concentration, and the density of the solute mass. The sum over all bins of the distribution provides the CCN/GCCN total number concentration and mass. Each table delineates between CCN and GCCN and contains 200 mass bins (from 10^{-19} to 10^{-8} g for CCN, and from 10^{-14} to 10^{-5} g for GCCN) and 14 possible median radii (from 0.01 to 0.96 μm for CCN, and from 1.5 to 5.5 μm for GCCN). Each distribution initially divides up the mass of only one CCN or GCCN (cm^{-3}) of a given size; thus, to obtain the true distribution at a grid point, each bin of the set distribution for one CCN is multiplied by the true number of nuclei that activate at a given time. The total mass, corresponding to the number of CCN, is determined by summing the mass in each bin of the distribution until this number is reached.

Cloud droplet formation takes place within the microphysics module if excess vapor exists and if the number of available nuclei that can activate is greater than the number of cloud droplets than nuclei. This prevents are ''soaking up'' of all excess vapor by potentially activated nuclei before vapor diffusion toward preexisting cloud droplets can take effect. As mentioned previously, it is assumed that 100% of GCCN can undergo growth by vapor diffusion in supersaturated conditions, regardless of other ambient conditions. The percentage of available CCN that can absorb excess vapor and form into cloud1 droplets is determined from the cloud droplet nucleation lookup table. Information concerning the temperature, vertical velocity, CCN concentration, and CCN median radius is fed into the lookup table, and an interpolated value is retrieved. This value is then multiplied by the number concentration of CCN located at the given grid point to determine the number of cloud droplets that form.

CCN and GCCN complete for vapor to form into cloud1 and cloud2 droplets, respectively. Excess vapor is diffused to each nuclei category based on the relative

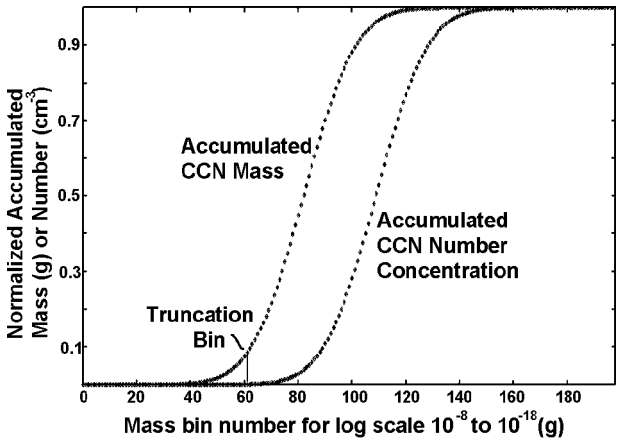

FIG. 4. The normalized accumulative mass and number bins for a CCN distribution. Note the differences between CCN mass and number accumulation within bins. This plot is for a CCN distribution with median radius = 0.16 μm.

ratio of the total surface area of all nuclei that can activate in each category. Given that the number concentration of CCN is typically from five to eight orders of magnitude greater than that for GCCN, only a relatively small amount of vapor is typically allotted toward droplet growth from GCCN, which allows GCCN to participate without consuming large amounts of excess vapor. GCCN have a large effect in terms of influencing collision–coalescence through the cloud2 mode without largely depleting the vapor supply to activated CCN.

It is assumed for both CCN and GCCN that the largest nuclei in each category activate first. The total mass that corresponds to the number of CCN is determined from the nuclei-spectrum lookup tables by summing the accumulated mass bins until the number is reached. Figure 4 shows sample normalized accumulated mass and number curves used for these calculations. Because mass begins significant accumulation before number, it leads to overdepletion of CCN mass. A truncation bin was introduced so that the mass distribution would be slightly altered and would not allow mass to be depleted before number. Mass and number are depleted from the nuclei source in the atmosphere and deposited in the variable that holds the nuclei mass contained within the cloud1 or cloud2 categories.

e. Nuclei mass transfer and restoration

Following the cloud droplet formation process, the CCN mass that is contained within hydrometeors must be tracked so as to restore the nuclei upon evaporation. This ''dissolved'' nuclei mass is transferred between hydrometeor holder categories whenever hydrometeors transfer between species. This is accomplished by transferring relative percentages of mass. For example, if 50% of the cloud1 mixing ratio is transferred to rain because of collisions with raindrops, then 50% of the dissolved CCN mass contained within the cloud1 category is transferred to the holder variable for rain. This transfer technique holds true for all possible transfers in the microphysics, including those resulting from collisions, melting, heterogeneous and homogeneous ice nucleation, and sedimentation. The scalar variables containing the dissolved aerosol mass are then allowed to advect and diffuse, similar to all other hydrometeor scalar variables. Fields of hydrometeor mass and dissolved aerosol mass remain highly correlated over time, with regions of maximum hydrometeor mass coinciding with maxima in dissolved aerosol mass.

During the vapor diffusion process, both evaporation and sublimation can take place if the air is subsaturated. It is assumed that, as liquid droplets evaporate, the dissolved nuclei mass begins to coagulate until it becomes a single dry mass once the entire hydrometeor has evaporated. Because the ice-phase hydrometeors sublimate, it is assumed that the dissolved, sub-CCN-sized particles are released back to the atmosphere but are too small to be significant for droplet formation. During evaporation, the percent of nuclei mass to restore is equal to the percentage of mixing ratio that evaporates from a given hydrometeor type. The RAMS mass–number lookup tables are used to calculate the number of evaporated liquid hydrometeors that corresponds to the lost mass; this number equals the number of restored nuclei. From the obtained mass and number, the nuclei median radius is computed. If the radius is less than (greater than) the threshold between CCN and GCCN, then the nuclei are added to the number concentration of CCN (GCCN).

4. Model tests with supercell simulations

Test simulations with the addition of the second cloud mode and prognostic cloud-number concentration were performed to examine model sensitivities to the new parameterizations and to compare the model responses with those expected from theory. These simulations were initialized as 3D, idealized, deep convective systems, using a homogeneous convective sounding (see Fig. 5) and a warm, moist bubble. The domain is 24 km in depth and 200 km in the horizontal direction. The vertical grid spacing varies from 100 m near the surface to 1 km above 10 km, and the horizontal spacing is 2 km. The warm bubble is 16 km wide and 2.5 km deep, with a temperature that is 3 K warmer than the environment and 20% more moist. The advantage of using a convective simulation is that the system is quasi steady, experiences a broad range of supersaturations, produces liquid and ice hydrometeors, and extends the model microphysics toward its physical limits. These simulations are a test of the robustness of the new parameterization, and no attempt is made to compare results with specific convective events.

These simulations were run with the one-moment version of the RAMS microphysics, with the following exception: two-moment prediction was turned on for pris-

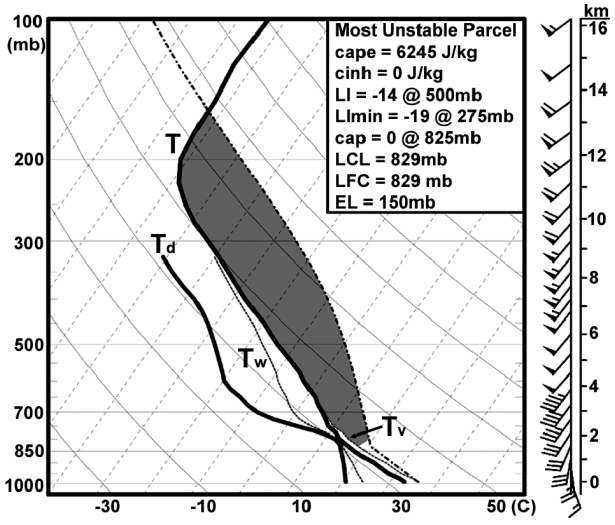

FIG. 5. Plot of the sounding used for initialization of the 3D, idealized, homogeneous, warm-bubble test simulations of the new microphysics parameterization. Profiles are temperature (T), dewpoint temperature (T_d), wet-bulb temperature (T_w), and virtual temperature (T_v). CAPE is computed within the shaded region.

tine ice in all simulations and for the cloud droplet modes when CCN or GCCN were allowed to activate. The microphysics was tested in terms of sensitivity to the large-cloud-droplet mode, number concentration of CCN and GCCN, and nuclei sources and sinks. The following analyses primarily focus on the influence of the large-droplet mode and activated nuclei on the mixing ratio and number concentrations of cloud droplets and pristine ice, as well as the in-cloud and surface-accumulated rainwater. All vertical cross sections that are discussed and displayed are analyzed as east–west cross sections through the central convective updraft at the chosen times. Model tests are summarized in Table 1.

a. Effects of the cloud2 category

The first simulations were performed to test the effects of the cloud2 mode as an additional hydrometeor species. Figure 6 reveals time series plots of the domain-averaged cloud1, cloud2, and rain spectra from a simulation designed as the 2D equivalent of the 3D simulation setup described above. This simulation had all three liquid hydrometeor types turned on with prognostic mixing ratio only. Spectrum curves are labeled sequentially at 3-min intervals, starting at 6 min into the simulation. Curve 1 represents the first model time step in which all three liquid hydrometeor types first appear simultaneously. Comparisons of the three spectra over time reveal the initial development of cloud1 and the lack of cloud2 and rain. By 9 min into the simulation (curve 2), cloud2 and rain begin to increase in number and size through autoconversion, at the expense of cloud1. Within 12 min (curve 3), the average rain spectrum has reached its peak at the expense of cloud1 and cloud2, whose curves display a marked decrease that coincides with development of rain. Curves 4 and 5 reveal a shift toward smaller sizes for cloud1 and cloud2 as further droplet formation occurs and the rain spectrum shifts to smaller sizes and decreases in number because of drop sedimentation.

Table 2 displays maxima in the accumulated rain at 30 min and in the cross sections of rain mixing ratio and pristine-ice number concentration at 60 min into the model runs. At 30 min into the simulations, the very presence of the cloud2 mode in experiment 2 has greatly reduced the amount of accumulated rainfall when compared with experiment 1. This relationship holds true when cloud1 has two predicted moments (expts 3 and 4) as well. There is also a reduction in rainfall for the two-moment prediction of cloud1 when compared with one-moment prediction (i.e., cf. expt 1 with expt 3 or exp2 with expt 4). The maxima in the cross sections of rain mixing ratio at 60 min into the model run were also examined. The inclusion of cloud2 in experiments 2 and 4 affects the rain category such that there is a large reduction in the overall maximum rain mixing ratio and a reduction in the horizontal and vertical range of influence of high-rain-mixing-ratio air. Comparisons between the one- and two-moment schemes of cloud1

TABLE 1. Summary of experiments for convective test simulations. For simulations containing CCN and/or GCCN, the respective median radii of the aerosol distributions are 0.04 and 3.0 μm.

Expt	Cloud1 moments	Cloud2 moments	CCN No. (cm^{-3})	GCCN No. (cm^{-3})	Sources and sinks
1	1	0	0	0	None
2	1	1	0	0	None
3	2	0	1000	0	None
4	2	1	1000	0	None
5	2	0	50	0	Source and sink
6	2	0	500	0	Source and sink
7	2	0	1000	0	Source and sink
8	2	2	1000	10^{-1}	None
9	2	2	50	10^{-1}	None
10	2	2	1000	10^{-5}	None
11	2	2	50	10^{-5}	None
12	2	0	1000	0	None
13	2	0	1000	0	Sink only
14	2	0	1000	0	Source and sink

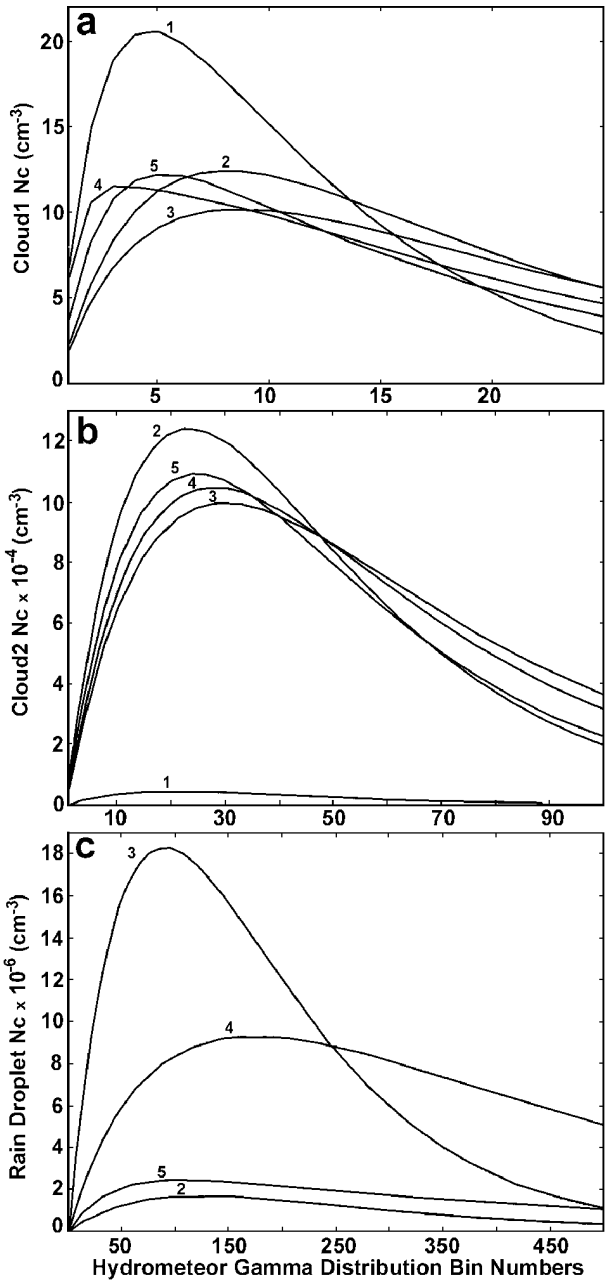

FIG. 6. Evolution of the (a) cloud1, (b) cloud2, and (c) rain spectra. Numbered curves are at 1) 360, 2) 540, 3) 720, 4) 900, and 5) 1080 s into a 2D warm-bubble simulation. The plotted spectra are domain averaged over all grid points that contain all three liquid hydrometeor types at the given model time step.

show slightly larger maxima in rain mixing ratio in the cloud created by the two-moment scheme; this observation complements the previous comparison in which the two-moment scheme produces a relative reduction in accumulated rainfall. Cross sections of the pristine-ice mixing ratio and number concentration at 60 min into the model runs reveal that the mixing ratio varies little among simulations but that the number concentration in experiments 1 and 2 is approximately 2 times that of experiments 3 and 4. The important decrease in ice crystal number in experiments 3 and 4 is due to the production of fewer, larger cloud1 droplets by parameterized CCN activation in the two-moment scheme. The one-moment diagnostic routine forces newly formed cloud droplets to exist initially with the smallest allowed radii; this allows for more numerous droplets to be present, which will freeze at a cold enough temperature to become part of the pristine-ice category.

TABLE 2. Results from sensitivity tests of the two cloud droplet modes and the number of predicted moments. Maximum domain values are given from fields of surface-accumulated rainfall at 30 min and from east–west vertical cross sections through the convective updraft of rain mixing ratio and pristine-ice number concentration at 60 min into the simulations.

Expt	Accumulated rainfall (mm)	Rain mixing ratio (g kg^{-1})	Pristine-ice No. concentration (cm^{-3})
1	32	4.7	81
2	18	2.7	72
3	24	5.2	36
4	15	3.1	43

b. Variations of CCN number concentration

In theory, initializing the model with fewer CCN should limit the number concentration of cloud1 droplets while still taking up a significant amount of vapor. With fewer CCN present in a supersaturated atmosphere, each nucleus can absorb a greater amount of vapor than if a large number of CCN are available (Pruppacher and Klett 1997). This vapor growth leads to the production of large cloud droplets that can initiate collection and rapidly grow to rain (Telford 1955; Berry 1967). These fewer, massive droplets rapidly reach a critical size and fall out of the cloud. Test simulations were run with varying number concentrations of CCN: experiments 5 (50 cm^{-3}), 6 (500 cm^{-3}), and 7 (1000 cm^{-3}). Table 3 displays resulting maxima in the accumulated rain at 120 min and in the cross sections of cloud1 and pristine-ice number concentration at 60 min into the model runs.

At 120 min into the simulation, there is a small but consistent decrease in the maximum total rainfall for a

TABLE 3. Results from sensitivity tests to the initial number concentration of CCN. Maximum domain values are given from fields of surface-accumulated rainfall at 120 min and from east–west vertical cross sections through the convective updraft of cloud1 number concentration and pristine-ice number concentration at 60 min into the simulations.

Expt	Accumulated rainfall (mm)	Cloud1 No. concentration (cm^{-3})	Pristine-ice No. concentration (cm^{-3})
5	43	50	19
6	41	330	31
7	37	700	22

TABLE 4. Results from sensitivity tests to the initial number concentration of CCN and GCCN. Maximum domain values are given from fields of surface-accumulated rainfall at 120 min and from east–west vertical cross sections through the convective updraft of cloud1 and cloud2 mixing ratio and number concentration at 60 min into the simulations.

Expt	Rainfall (mm)	Cloud1 mixing ratio (g kg^{-1})	Cloud1 No. concentration (cm^{-3})	Cloud2 mixing ratio (g kg^{-1})	Cloud2 No. concentration (cm^{-3})
8	30	3.2	850	0.045	0.36
9	35	3.0	70	0.110	0.43
10	26	3.5	830	0.031	0.36
11	34	3.1	77	<0.010	<0.10

corresponding increase in the number concentration of CCN for experiments 5–7. Between simulations, the greatest decrease occurs between experiments 6 and 7 as CCN number approaches 1000 cm^{-3}. Because CCN are activated in the model, there is such an abundance of them in experiment 7 that initially few are able to absorb enough vapor to grow to the cloud1 droplet sizes that have substantial collection efficiencies; thus, as expected, a greater CCN number slows the droplet spectrum broadening process. Values of cloud1 number concentration reveal the direct impact of increasing CCN number. For an increasing number of initial CCN, the cloud1 number concentration is increased, but there is a relative decrease in the percent of CCN that activate to form cloud droplets. This process is limited by the amount of excess vapor that is available when cloud1 droplet formation occurs and by the minimum threshold for cloud1 droplet size. Pristine ice is influenced such that an increase in initial CCN corresponds indirectly to an increase in ice crystal number, though the greatest number of crystals appears for the midrange value of initial CCN number. Further investigation reveals that the temperature regime necessary for activation of the Hallett–Mossop process exists in a layer just below a region of high concentration of pristine ice (~8500 m) and in a region of large vertical velocity. The number of cloud droplets with diameters less than 13 and greater than 24 μm, which is needed for ideal ice splintering, is maximized for the initial midrange value of CCN number in experiment 6. Experiments 5 and 7 produce fewer, larger droplets and many, smaller droplets, respectively, such that the preferential distribution of cloud droplets needed for secondary ice production is not maximized.

c. Variations of GCCN number concentration

Both CCN and GCCN, with median radii of 0.04 and 3.0 μm, respectively, were allowed to vary their initial number concentration to test the relative sensitivity to one another. Table 4 displays resulting maxima in the accumulated rain at 120 min and in the cross sections of cloud1 and cloud2 number concentration at 60 min into the model runs. The rainfall patterns are very similar among simulations, but the maximum rainfall varies by up to nearly 30% from the greatest to least accumulation. There is generally an increase in the rainfall for a decrease in initial CCN and a constant number of GCCN, with the greatest increase occurring between experiments 10 and 11 when the fewest initial GCCN are present. When the number of CCN is held constant and is small (large) and GCCN number are allowed to vary, the result is a relatively small (large) increase in total rainfall for an increase in GCCN number. The greatest total rainfall occurs for experiments 9 and 11 with the fewest CCN, because many of these nuclei, along with the GCCN, result in the formation of large droplets that experience rapid collisional growth into rain. For experiments 8 and 10 with many CCN, the GCCN have a greater impact on rain production because the cloud1 category is inundated with many small cloud droplets that require more time to reach raindrop sizes. Feingold et al. (1999), Woodcock et al. (1971), and Takahashi (1976) also found that GCCN are most influential in rain production in continental clouds in which precipitation processes occur slowly in comparison with such processes in maritime clouds.

Despite large differences among the initial nuclei numbers in these simulations, the cloud1 mixing ratio varies only slightly, and the greatest difference in number concentration is due to the difference in the number of initial CCN. There is only a slight reduction in cloud1 number as the number of GCCN is increased. This moderate reduction is due to the competition for vapor that occurs in the cloud nucleation routine. The differences in the mixing ratio and number concentration of the cloud2 mode are more dramatic than those of the cloud1 mode. The largest (smallest) magnitude in mixing ratio and number of cloud2 occurs in experiment 9 (expt 11) with few CCN and many (few) GCCN. The differences in maxima are less dramatic when a large number of CCN are present, though the mixing ratio of cloud2 is slightly greater for a greater number of GCCN. The corresponding number concentrations are more similar, which is attributed to collisional growth of cloud1 droplets to cloud2 sizes; such growth initially adds more number than mass.

d. Introduction of CCN and GCCN sources and sinks

Tests were also performed to examine the influence of CCN and GCCN depletion at the time of nucleation and also the restoration of nuclei upon evaporation of liquid hydrometeors. Figure 7 displays cross sections of cloud1 number concentration for these simulations. Experiment 12 (expt 13) contains the highest (lowest) concentration of cloud droplets at 60 min into the simulation, and experiment 14 displays number concentrations, throughout the cross section, that are slightly higher than experiment 13. Evaporation of liquid droplets is influential in experiment 14 by providing restored CCN to regions of the storm that can reactivate CCN

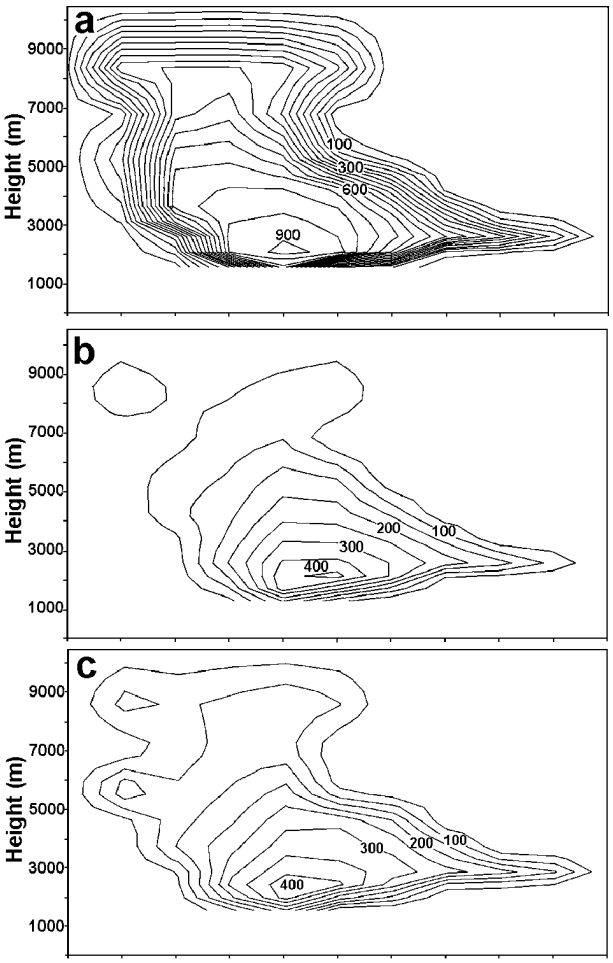

FIG. 7. Cross section of cloud droplet number concentration (cm^{-3}) at 60 min into the simulations for the following model run conditions: (a) no CCN sources or sinks, (b) only CCN depletion upon nucleation, and (c) CCN depletion upon nucleation and restoration upon evaporation of liquid hydrometeors. Horizontal tick marks are 2 km apart.

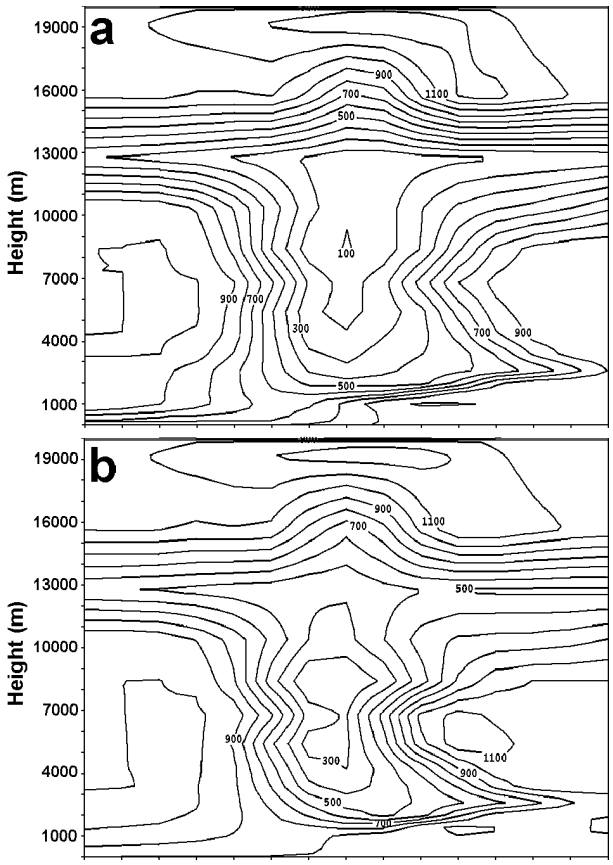

FIG. 8. Cross section of CCN number concentration (cm^{-3}) at 60 min into the simulations for the following model run conditions: (a) only CCN depletion upon nucleation and (b) CCN depletion upon nucleation and restoration upon evaporation of liquid hydrometeors. Horizontal tick marks are 2 km apart.

to form cloud droplets and maintain a relatively higher number concentration of cloud1.

The corresponding cross section of CCN number concentration in Fig. 8 reveals a number of interesting effects that the convection has upon the field of CCN. Recall that experiment 12 has a nonchanging CCN field over time and so is not shown. Experiments 13 and 14 reveal a domain maximum of 1200 CCN cm^{-3}, located just above the main updraft along the top of the anvil. These values are above the initial concentration of 1000 cm^{-3} and are a result of convergence of CCN-rich air over the updraft. The minimum values are located within the central updraft in the storm and in the region of low-level entrainment just ahead of the updraft. Experiment 14 contains a similar pattern to that of experiment 13 but with zones of enhanced CCN concentration in regions of maximum evaporation. In experiment 14, CCN concentrations of 200–300 cm^{-3} higher than experiment 13 are found below and to the rear of the center of the storm and in advance of the storm in a region of midlevel entrainment.

5. Conclusions

The CSU RAMS bulk microphysics has been upgraded to include a second mode of cloud droplets with a 40–80-μm range in diameter. The inclusion of the second mode better represents the two modes that exist naturally in many environments. The large-droplet mode is shown to slow the process of rain development and/or reduce the total amount of rainfall relative to only a single mode. Accompanying this upgrade is the development of prognostic number concentration of two cloud droplet modes through the activation of CCN and GCCN and growth by vapor diffusion. Activation of CCN, for nucleation of cloud1 droplets, is possible through a series of nucleation lookup tables that were created by a Lagrangian parcel model that is based upon the Köhler equations. Lookup tables contain the percentage of CCN to nucleate, depending upon atmospheric temperature, vertical velocity, number concen-

tration of CCN, and the median radius of CCN. The parcel model revealed that nearly all GCCN are activated for any reasonable range of atmospheric condition, and so tables are not needed for the formation of cloud2 droplets from GCCN. The model user has the freedom to specify the initial fields of CCN and GCCN concentration and the median radius of the nuclei. An option is also available to run the model with no CCN sources or sink, sinks only, or both sources and sinks. CCN mass and number can be removed upon droplet formation, and the mass is tracked within the hydrometeor species; this mass and corresponding number concentration can be restored upon evaporation of liquid hydrometeors. The largest nuclei are activated first, resulting in a shift in the nuclei spectrum and the median radius, which influences the percent that are activated at the following time step.

A dynamic warm-bubble simulation was used for testing because it encompasses a wide range of temperatures, vertical velocities, supersaturations, and hydrometeor types. Test results were analyzed for model sensitivity and for comparison with results expected from theory. The following list summarizes the overall sensitivities as they apply to these simulations:

1) Introduction of the cloud2 mode slows and reduces the production of rain by acting as an intermediate hydrometeor category between cloud1 and rain.
2) Increasing the number concentration of CCN results in an increase in the number concentration and mixing ratio of the cloud1 mode, which, in turn, reduces the surface accumulation of rain.
3) Increasing the number concentration of GCCN results in an increase in the number concentration and mixing ratio of the cloud2 mode. This increase also produces an increase in the surface accumulation of rain. The impact of GCCN on rainfall variation is maximized in situations where a large number of CCN are present, and their impact on the cloud2 mode is maximized in situations in which few CCN are present.
4) The depletion of CCN upon nucleation reduces the overall mass and number of cloud1 droplets and increases rainfall, as compared with the simulation with a nonchanging, homogeneous field of CCN. As compared with the case with only CCN sink terms, the case with both sink and evaporative source terms results in a relative increase in CCN near the surface and to the front and rear of the convective cell in regions of enhanced evaporation.

Further simulations involving less vigorous systems will be used to test more comprehensively the robustness of the RAMS improvements. Icing simulations are under way for a case, occurring from 29 to 30 January 1998, that has been documented and modeled and in which aircraft measurements were taken (results to be presented in forthcoming work). These simulations will be used to test further the new model parameterizations and to examine the links among CCN activation, the large-cloud-droplet mode, and ice formation. These influences are likely of great importance in the challenge of forecasting aircraft-icing events.

Acknowledgments. This research was supported by a grant from the National Center for Atmospheric Research under Grant S00-19852 and by the National Science Foundation under Grant ATM-9900929. We thank Bob Walko of Atmet, Inc., for his consulting and assistance with the RAMS microphysics code and Lagrangian parcel model. We also thank Graham Feingold of NOAA/ETL for providing and assisting with the parcel model and for his expertise in the treatment of nuclei in cloud modeling. This research is in response to requirements and funding by the Federal Aviation Administration (FAA). The views expressed are those of the authors and do not necessarily represent the official policy or position of the FAA.

REFERENCES

Berry, E. X., 1967: Cloud droplet growth by collection. *J. Atmos. Sci.,* **24,** 688–701.

——, 1968: Comments on ''Cloud droplet coalescence: Statistical foundations and a one-dimensional sedimentation model.'' *J. Atmos. Sci.,* **25,** 151–152.

——, and R. L. Reinhardt, 1974: An analysis of cloud drop growth by collection: Part IV. A new parameterization. *J. Atmos. Sci.,* **31,** 2127–2135.

Brown, P. N., G. D. Byrne, and A. C. Hindmarsh, 1989: VODE: A variable coefficient ODE solver. *SIAM J. Sci. Stat. Comput.,* **10,** 1038–1051.

Clark, T. L., 1976: Use of log-normal distributions for numerical calculations of condensation and collection. *J. Atmos. Sci.,* **33,** 810–821.

——, and W. D. Hall, 1983: A cloud physical parameterization method using movable basis functions: Stochastic coalescence parcel calculations. *J. Atmos. Sci.,* **40,** 1709–1728.

Cooper, W. A., R. T. Bruintjes, and G. K. Mather, 1997: Calculations pertaining to hygroscopic seeding with flares. *J. Appl. Meteor.,* **36,** 1449–1469.

Cotton, W. R., 1972: Numerical simulation of precipitation development in supercooled cumuli—Part I. *Mon. Wea. Rev.,* **100,** 757–763.

——, and Coauthors, 2003: RAMS 2001: Current status and future directions. *Meteor. Atmos. Phys.,* **82,** 5–29.

Dudhia, J., 1989: Numerical study of convection observed during the winter monsoon experiment using a mesoscale two-dimensional model. *J. Atmos. Sci.,* **46,** 3077–3107.

Feingold, G., and A. J. Heymsfield, 1992: Parameterizations of condensational growth of droplets for use in general circulation models. *J. Atmos. Sci.,* **49,** 2325–2342.

——, S. Tzivion, and Z. Levin, 1988: Evolution of raindrop spectra. Part I: Solution to the stochastic collection/breakup equation using the method of moments. *J. Atmos. Sci.,* **45,** 3387–3399.

——, W. Cotton, S. Kreidenweis, and J. Davis, 1999: The impact of giant cloud condensation nuclei on drizzle formation in stratocumulus: Implications for cloud radiative properties. *J. Atmos. Sci.,* **56,** 4100–4117.

Ferrier, B. S., W. K. Tao, and J. Simpson, 1995: A double-moment multiple-phase four-class bulk ice scheme. Part II: Simulations of convective storms in different large-scale environments and comparisons with other bulk parameterizations. *J. Atmos. Sci.,* **52,** 1001–1033.

Hall, W., 1980: A detailed microphysical model within a two-di-

mensional dynamic framework: Model description and preliminary results. *J. Atmos. Sci.,* **37,** 2486–2507.
Hallett, J., and S. C. Mossop, 1974: Production of secondary ice crystals during the riming process. *Nature,* **249,** 26–28.
Heymsfield, A. J., and R. M. Sabin, 1989: Cirrus crystal nucleation by homogeneous freezing of solution droplets. *J. Atmos. Sci.,* **46,** 2252–2264.
Hobbs, P. V., M. K. Politovich, and L. F. Radke, 1980: The structures of summer convective clouds in eastern Montana. I: Natural clouds. *J. Appl. Meteor.,* **19,** 645–663.
Hong, S. Y., H. M. H. Juang, and O. Zhao, 1998: Implementation of prognostic cloud scheme for a regional spectral model. *Mon. Wea. Rev.,* **126,** 2621–2639.
Hsie, E. Y., and R. A. Anthes, 1984: Simulations of frontogenesis in a moist atmosphere using alternative parameterizations of condensation and precipitation. *J. Atmos. Sci.,* **41,** 2701–2716.
Johnson, D. B., 1982: The role of giant and ultragiant aerosol particles in warm rain initiation. *J. Atmos. Sci.,* **39,** 448–460.
Kessler, E., 1969: *On the Distribution and Continuity of Water Substance in Atmospheric Circulation. Meteor. Monogr.,* No. 32, Amer. Meteor. Soc., 84 pp.
Khairoutdinov, M., and Y. L. Kogan, 2000: A new cloud physics parameterization in a large-eddy simulation model of marine stratocumulus. *Mon. Wea. Rev.,* **128,** 229–243.
Kogan, Y. L., 1991: The simulation of a convective cloud in a 3-D model with explicit microphysics. Part I: Model description and sensitivity experiments. *J. Atmos. Sci.,* **48,** 1160–1189.
Lin, Y. L., R. D. Farley, and H. D. Orville, 1983: Bulk parameterization of the snow field in a cloud model. *J. Climate Appl. Meteor.,* **22,** 1065–1092.
Long, A., 1974: Solutions to the droplet collection equation for polynomial kernels. *J. Atmos. Sci.,* **31,** 1040–1052.
Low, R., 1969: A generalized equation for the solution effect in droplet growth. *J. Atmos. Sci.,* **26,** 608–611.
Manton, M. J., and W. R. Cotton, 1977: Parameterization of the atmospheric surface layer. *J. Atmos. Sci.,* **34,** 331–334.
Meyers, M. P., R. L. Walko, J. Y. Harrington, and W. R. Cotton, 1997: New RAMS cloud microphysics parameterization. Part II. The two-moment scheme. *Atmos. Res.,* **45,** 3–39.
Mossop, S. C., 1978: The influence of drop size distribution on the production of secondary ice particles during graupel growth. *Quart. J. Roy. Meteor. Soc.,* **104,** 323–330.
Ovtchinnikov, M., and Y. L. Kogan, 2000: An investigation of ice production mechanisms in small cumuliform clouds using a 3D model with explicit microphysics. Part I: Model description. *J. Atmos. Sci.,* **57,** 2989–3003.
Pruppacher, H., and J. Klett, 1997: *Microphysics of Clouds and Precipitation,* 2d ed. Vol. 18, Kluwer Academic, 954 pp.
Reisner, J., R. M. Rasmussen, and R. T. Bruintjes, 1998: Explicit forecasting of supercooled liquid water in winter storms using the MM5 mesoscale model. *Quart. J. Roy. Meteor. Soc.,* **124,** 1071–1107.
Rutledge, S. A., and P. V. Hobbs, 1983: The mesoscale and microscale structure and organization of clouds and precipitation in midlatitude cyclones. VIII: A model for the ''seeder-feeder'' process in warm-frontal rainbands. *J. Atmos. Sci.,* **40,** 1185–1206.
Souto, M. J., C. F. Balseiro, V. Pérez-Muñuzuri, M. Xue, and K. Brewster, 2003: Impact of cloud analysis on numerical weather prediction in the Galician region of Spain. *J. Appl. Meteor.,* **42,** 129–140.
Takahashi, T., 1976: Warm rain, giant nuclei and chemical balance—A numerical model. *J. Atmos. Sci.,* **33,** 269–286.
Tao, W. K., J. Simpson, and M. McCumber, 1989: An ice-water saturation adjustment. *Mon. Wea. Rev.,* **117,** 231–235.
Telford, J. W., 1955: A new aspect of coalescence theory. *J. Atmos. Sci.,* **12,** 436–444.
Tzivion, S., G. Feingold, and Z. Levin, 1987: An efficient numerical solution to the stochastic collection equation. *J. Atmos. Sci.,* **44,** 3139–3149.
——, T. Reisin, and Z. Levin, 1994: Numerical simulation of hygroscopic seeding in a convective cloud. *J. Appl. Meteor.,* **33,** 252–267.
Verlinde, J., P. J. Flatau, and W. R. Cotton, 1990: Analytical solutions to the collection growth equation: Comparison with approximate methods and application to cloud microphysics parameterization schemes. *J. Atmos. Sci.,* **47,** 2871–2880.
Walko, R. L., W. R. Cotton, M. P. Meyers, and J. Y. Harrington, 1995: New RAMS cloud microphysics parameterization: Part I. The single-moment scheme. *Atmos. Res.,* **38,** 29–62.
——, ——, ——, and ——, 2000: Efficient computation of vapor and heat diffusion between hydrometeors in a numerical model. *Atmos. Res.,* **53,** 171–183.
Woodcock, A. H., R. A. Duce, and J. L. Moyers, 1971: Salt particles and raindrops in Hawaii. *J. Atmos. Sci.,* **28,** 1252–1257.
Zhao, Q., and F. H. Carr, 1997: A prognostic cloud scheme for operational NWP models. *Mon. Wea. Rev.,* **125,** 1931–1953.